PHYSICAL REVIEW C VOLUME 23, NUMBER 1 JANUARY 1981

Elastic and inelastic scattering measurements for the $^{24}Mg+^{208}Pb$ and $^{28}Si+^{208}Pb$ systems

J. S. Eck
The Australian National University, Canberra, ACT 2600, Australia
and Kansas State University, Manhattan, Kansas 66506

T. R. Ophel, P. D. Clark, and D. C. Weisser
The Australian National University, Canberra, ACT 2600, Australia

G. R. Satchler
Oak Ridge National Laboratory, Oak Ridge, Tennessee 37830
(Received 24 April 1980)

The measurement and analysis of the differential cross sections for the elastic and inelastic scattering to the lowest 2^+ states of ^{24}Mg and ^{28}Si using ^{24}Mg and ^{28}Si beams in conjunction with ^{208}Pb targets are reported. The incident beam energies were 145 MeV for ^{24}Mg and 162 MeV for ^{28}Si. The measured cross sections were analyzed using coupled channels calculations assuming a rotational model description for the low-lying collective states of ^{24}Mg and ^{28}Si. The coupled channels calculations are compared with polarization potential calculations in which the experimental $B(E2)$ values are used in both cases. The extracted deformation lengths and deformation parameters are compared to those obtained using similar data with light projectiles, although because of strong Coulomb excitation the present calculations are fairly insensitive to the nuclear deformation parameters.

[NUCLEAR REACTIONS $^{208}Pb(^{24}Mg,^{24}Mg)$, $^{208}Pb(^{24}Mg,^{24}Mg^*)$ $Q=-1.37$ MeV, $E=145$ MeV; $^{208}Pb(^{28}Si,^{28}Si)$, $^{208}Pb(^{28}Si,^{28}Si^*)$ $Q=-1.78$ MeV, $E=162$ MeV, measured $\sigma(\theta)$, $\theta_{lab}=20-120°$; optical model calculations including polarization potential, coupled channels calculations, extracted deformation parameters.]

I. INTRODUCTION

In the last decade there has been an increased interest in nuclear heavy ion inelastic scattering measurements and the extraction of nuclear deformation parameters from these data.[1-7] Investigations of inelastic scattering from ^{24}Mg and ^{28}Si using strongly interacting projectiles ranging in mass from $A=1-16$ have shown that (a) the nuclear potential and charge deformations for these nuclei are essentially equal within the validity of the rotational model, and (b) the effects of the finite projectile size Δ in the extraction of the nuclear potential shape can be accounted for geometrically[8,9] using a simple model proposed by Hendrie.

In the present work we have investigated the scattering and excitation of ^{24}Mg and ^{28}Si when they interact with a very heavy nucleus, ^{208}Pb. In these cases the "projectile" size (i.e., the size of the ^{208}Pb) is twice that of the nucleus being excited and the Coulomb interaction is very strong, making the effect of Coulomb excitation extremely important in the measured cross sections. The effects of Coulomb and nuclear excitation on the elastic cross sections are investigated using an optical model which includes a polarization term in the imaginary potential[10] and both elastic and inelastic cross sections are calculated using coupled channels calculations (CC) based on a rotational model description of the low-lying states of ^{24}Mg and ^{28}Si. The experimental details are given in Sec. II, the polarization potential and CC calculations are described in Sec. III, the extraction of the deformation parameters for ^{24}Mg and ^{28}Si and their dependence on projectile size are discussed in Sec. IV, and the results and conclusions of the present study are summarized in Sec. V.

II. EXPERIMENTAL PROCEDURE

The ^{28}Si beam was obtained from the Australian National University sputter ion source as $^{28}Si^-$ and was accelerated using the 14UD tandem Van de Graaff accelerator. The ions were stripped twice. The first stripping occurred at the terminal and the second stripping occurred at a distance down from the terminal of one-third the length of the high energy tube. The energy selection magnet was set to allow transmission of the $1^- \rightarrow 9^+ \rightarrow 12^+$ beam through to the scattering chamber. A beam intensity of 40–60 nA was obtained. The ^{24}Mg beam was obtained in a similar manner except that only single stripping at the terminal was employed. The energy selection magnet was set to allow transmission of the 10^+ beam to the target and a beam current of 40 nA was achieved. The targets consisted of ^{208}Pb (~40–100 $\mu g/cm^2$) evaporated onto thin carbon foils. The scattered ^{28}Si and ^{24}Mg projectiles were detected using the Enge split pole

spectrometer and focal plane detector.[11] The focal plane detector was operated in the heavy ion mode[11] and therefore contributions from the various charge states were added in determining the total scattered yield. Typical position spectra gated on the appropriate mass window are shown in Fig. 1 for both $^{24}Mg + ^{208}Pb$ and $^{28}Si + ^{208}Pb$. In the case of $^{24}Mg + ^{208}Pb$ the 1.37 MeV state of ^{24}Mg is well resolved from the 2.61 MeV state of ^{208}Pb, while for $^{28}Si + ^{208}Pb$ the 1.78 MeV state of ^{28}Si is not completely resolved from the 2.61 MeV state of ^{208}Pb. Coulomb excitation calculations indicate, however, that the excitation of the 3^- (2.61 MeV) state in Pb is less than 10% that of the 2^+ (1.78 MeV) state in ^{28}Si for all the angles studied here. Excitation of the 4^+ states in either ^{24}Mg or ^{28}Si was detectable at some angles but, in general, was quite small. All significant charge states could be detected simultaneously on the focal plane using the present setup. The relative normalization was obtained using a monitor detector placed at 15° with respect to the beam. The absolute normalization was obtained by assuming that the forward angle elastic scattering cross sections are pure Rutherford scattering. This assumption appears to be strongly valid and the absolute cross sections are accurate to 10%. The measured cross sections for scattering to the ground and lowest 2^+ states in ^{28}Si and ^{24}Mg are shown in Figs. 2 and 3, respectively. Only statistical errors are indicated in the figures. The elastic scattering cross sections are pure Rutherford scattering at very forward angles ($\theta_{c.m.} \lesssim 40°$), show a slow falloff with angle at intermediate angles ($40° \lesssim \theta_{c.m.} \lesssim 80°$) due to the onset of strong Coulomb excitation, and finally at backward angles ($\theta_{c.m.} \lesssim 90$) the cross sections fall steeply with angle due to the onset of strong nuclear absorption processes.

III. ANALYSIS

The angular distributions were initially analyzed using an optical model potential to which was added an imaginary polarization potential in order to account for the strong Coulomb excitation processes which remove flux from the elastic channel even

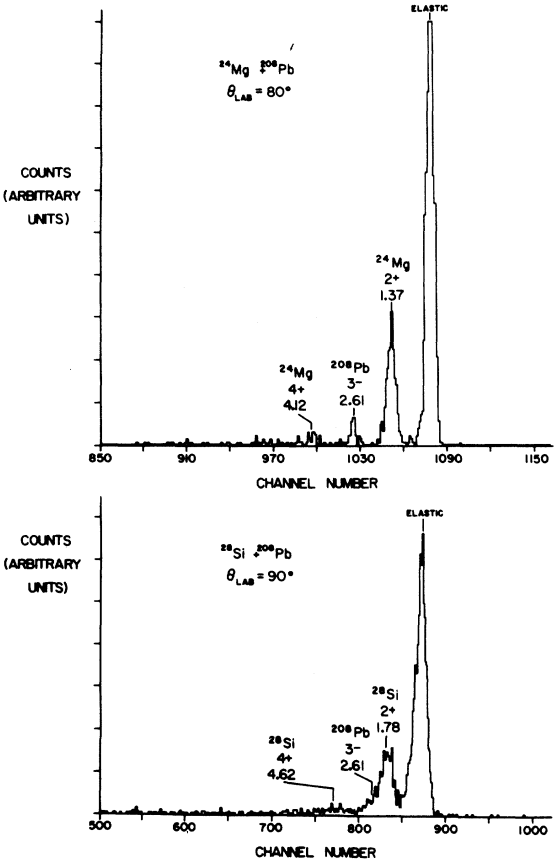

FIG. 1. Position spectra gated on projectile mass for $^{24}Mg + ^{208}Pb$ at $\theta_{lab} = 80°$ and $E_{lab} = 145$ MeV (top) and $^{28}Si + ^{208}Pb$ at $\theta_{lab} = 90°$ and $E_{lab} = 162$ MeV (bottom).

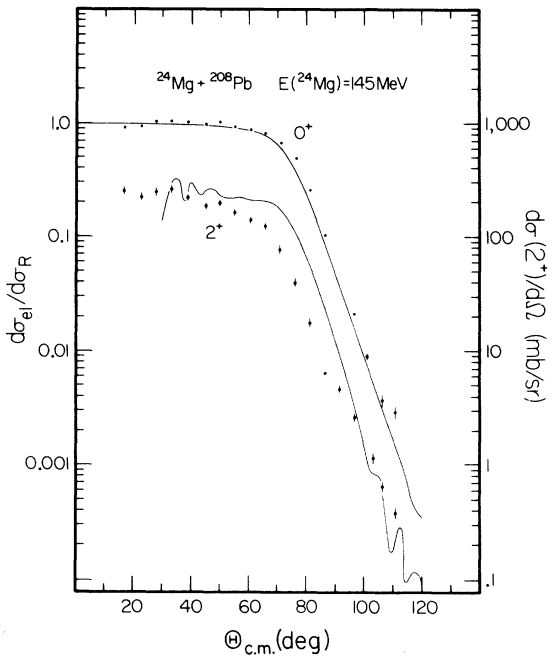

FIG. 2. Elastic and inelastic scattering angular distributions for the $^{24}Mg + ^{208}Pb$ system at $E_{lab} = 145$ MeV. The elastic scattering is shown as the ratio to Rutherford and is given by the left hand scale while the inelastic cross section is plotted in units of (mb/sr) and is shown by the right hand scale. The measured cross sections are indicated by the dots. The solid curves are coupled channels calculations using the optical model parameters of Table I, the experimental value of $B(E2)$, and for a value of the nuclear deformation parameter $\beta_2^n = 0.0$. See text for details.

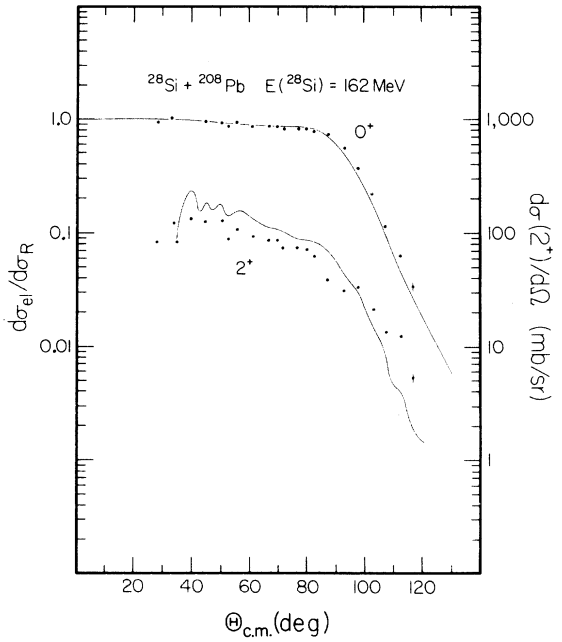

FIG. 3. Elastic and inelastic scattering angular distributions for the ^{28}Si+^{208}Pb system at E_{lab}=162 MeV. The elastic scattering is shown as the ratio to Rutherford and is given by the left hand scale while the inelastic cross section is plotted in units of (mb/sr) and is shown by the right hand scale. The measured cross sections are indicated by the dots. The solid curves are coupled channels calculations using the optical model parameters of Table I, the experimental value of $B(E2)$, and a value of the nuclear deformation parameter β_2^n = 0.0. See text for details.

for large impact parameters. The optical potential plus polarization potential[10] is given by

$$U(R) = (V + iW)f(R) + i\,\mathrm{Im}U_p(R) + V_c(R),$$

$$f(r) = \frac{1}{1+\exp(R-R_0)/a}, \qquad (1)$$

$$R_0 = r_0(A_t^{1/3} + A_p^{1/3}),$$

where r_0 is the radius parameter and a is the diffuseness parameter. The same geometrical parameters were used for both the real and imaginary potentials. The Coulomb potential $V_c(R)$ is that of a uniformly charged sphere of radius R_c and is given by

$$V_c(R) = \frac{Z_1 Z_2 e^2}{2R_c}\left[3 - \left(\frac{R}{R_c}\right)^2\right], \quad R \lesssim R_c$$

$$= \frac{Z_1 Z_2 e^2}{R}, \quad R > R_c. \qquad (2)$$

The polarization potential $U_p(R)$ is calculated using the formalism of Love *et al.*[10] In the present work only quadrupole excitation is considered and the imaginary part of the polarization potential for quadrupole Coulomb excitation is given by[10]

$$\mathrm{Im}U_p(R) = -\left[1 - \frac{2}{7}\left(\frac{R_c}{R}\right)^2 - \frac{1}{21}\left(\frac{R_c}{R}\right)\right]K_C(R)\frac{W_p}{R^5}, \quad R \gtrsim R_c$$

$$= -\tfrac{2}{3}K_c\frac{W_p R^4}{R_c^{\,9}}, \quad R < R_c, \qquad (3)$$

where

$$K_c(R) = \left(1 - \frac{Z_t Z_p e^2}{R E_{c.m.}}\right)^{-1/2}. \qquad (4)$$

The polarization strength W_p is given by

$$W_p = 0.01676\frac{\mu Z_p^{\,2}}{k}B(E2, 0 \to 2)g_2(\xi)\ \mathrm{MeV\,fm^5}, \qquad (5)$$

where the reduced mass μ is in u, the wave number k in fm^{-1}, and the $B(E2)$ in e^2 fm^4 units.[10]

In fitting the elastic cross section angular distributions, the real potential strength V was set equal to 40 MeV, and the radius parameter r_0, which was the same for all potentials, was set equal to 1.3 fm. The polarization potential W_p was calculated using the experimental values[12,13] for $B(E2, 0 \to 2)$, $B(E2)$=420 e^2fm^4 and 320 e^2fm^4 for the first 2$^+$ states in ^{24}Mg and ^{28}Si, respectively. Only the Woods-Saxon imaginary well strength W and the diffuseness parameter a were varied to obtain the best fits. The best fit values of the

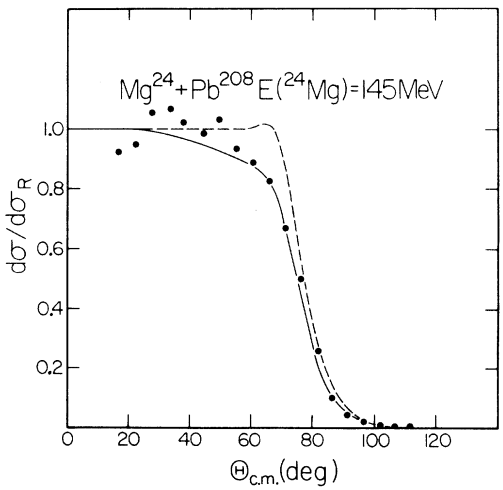

FIG. 4. Elastic scattering angular distribution for ^{24}Mg+^{208}Pb at E_{lab}=145 MeV plotted on a linear scale as the ratio-to-Rutherford scattering. The measured cross sections are indicated by dots. The solid curve is the optical model fit including the polarization potential calculated using the parameters of Table I. The dashed curve is the same optical model calculation but does not include any polarization contribution (i.e., U_p=0). See text for details.

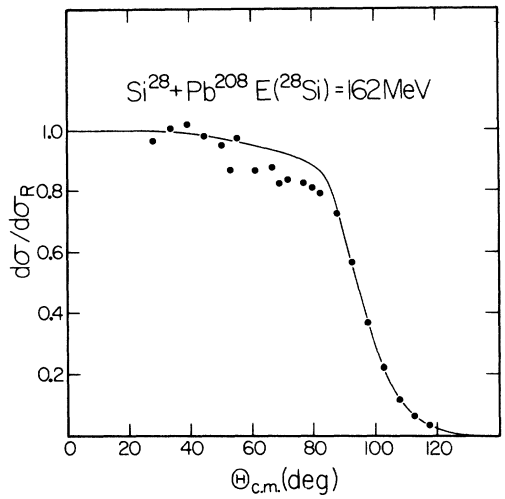

FIG. 5. Elastic scattering angular distribution for $^{28}Si+^{208}Pb$ at $E_{lab}=162$ MeV plotted on a linear scale as the ratio-to-Rutherford scattering. The measured cross sections are indicated by dots. The solid curve is the optical model fit including the polarization potential calculated using the parameters of Table I. See text for details.

parameters are given in Table I and the calculated cross sections are shown in Figs. 4 and 5 for $^{24}Mg+^{208}Pb$ and $^{28}Si+^{208}Pb$, respectively. (Note that the cross sections in Figs. 4 and 5 are plotted on a linear scale.) Also shown for the $^{24}Mg+^{208}Pb$ angular distribution is the calculation with the polarization potential U_p set equal to zero. For the $^{24}Mg+^{208}Pb$ the calculated cross section describes the data well if the polarization potential is included. This shows that Coulomb excitation is important in removing flux at large impact parameters (small scattering angles) and produces a considerable effect on the elastic scattering cross sections. For the case of $^{28}Si+^{208}Pb$ the calculated cross section lies consistently higher than the measured cross sections. The effect of Coulomb excitation on the elastic scattering cross section is considerable for the case of $^{28}Si+^{208}Pb$ also, but apparently does not account fully for the decrease from Rutherford scattering in the intermediate angular range. This effect will be investigated further utilizing the coupled channels calculations.

The real well-depth V was also varied (together with W and a) in an attempt to improve the fits. No significant improvement was obtained. What did emerge was that these data are rather insensitive to the real potential.

Real potentials were also generated from the folding model for these systems, using the $M3Y$ interaction which has successfully accounted for the real potential for many other heavy ion systems.[14] As described elsewhere,[14] densities based upon electron scattering were used for ^{24}Mg and ^{28}Si, while Negele's Hartree-Fock density was used for ^{208}Pb. Rather than use them directly, Woods-Saxon potentials were obtained which closely fitted the folded ones over the range $R=11-16$ fm, which is important for the present data. These had $r_0=1.25$ fm, $a=0.63$ fm, and $V=36.1$ MeV ($^{24}Mg+^{208}Pb$) and 35.1 MeV ($^{28}Si+^{208}Pb$). A phenomenological Woods-Saxon imaginary potential with $r_w=1.3$ fm was added, in the usual way, together with the polarization potential U_p. The imaginary strength W and diffuseness a_w were varied to fit the data. Fits were found equivalent to those obtained before with $W=174$ MeV, $a_w=0.480$ fm for $^{24}Mg+^{208}Pb$ and with $W=206$ MeV, $a_w=0.308$ fm for $^{28}Si+^{208}Pb$.

Arbitrarily varying the strength of the real, folded, potential did not result in any improvement, but demonstrated again that the data fits are insensitive to the real potential. Hence we can only conclude that the data are *compatible* with the usual folding model. It would appear that higher energies are required before the shielding effects of the long-range, absorbing, polarization potential are overcome and the scattering becomes more sensitive to the real potential.

It does seem that the "nuclear" part of the imaginary potential is rather better determined; this part of the potential is required to produce the onset of the shadow region, the sudden drop of the cross section below the Rutherford value. For example, at $R=13$ fm, which is close to the strong absorption radius, the fits to the ^{24}Mg data consistently demand that $\mathrm{Im}U\approx -7$ MeV. The value for ^{28}Si at $R=13$ fm is less well-determined but is about $-(3\pm0.5)$ MeV. These are surprisingly

TABLE I. Optical model parameter sets used in polarization potential and coupled channels calculations. Underlined parameters were initially fixed and not varied in any of the optical model fitting procedures.

	E_{lab} (MeV)	V (MeV)	W (MeV)	r_0 (fm)	a (fm)	W_p (MeV fm^5)	σ_R (mb)
$^{24}Mg+^{208}Pb$	145	<u>40.0</u>	188.0	<u>1.3</u>	0.481	4.91×10^4	2060
$^{28}Si+^{208}Pb$	162	<u>40.0</u>	152.0	<u>1.3</u>	0.361	2.39×10^4	1095

large values; most other systems studied,[14] including the not too dissimilar[1] $^{20}Ne + ^{208}Pb$ at 131 MeV, yield values of around 1 MeV, although there is a tendency for these to increase as the systems become heavier. Further, because of the long-range Coulomb excitation, the strong-absorption radius is not very well defined in the present cases.

At least for the potentials explored here, the imaginary part is several times stronger than the real part. This is also in contrast with other systems studied, where the two parts are usually comparable near the strong-absorption radii. For example, the case[1] of $^{20}Ne + ^{208}Pb$ at 131 MeV yields an imaginary potential which is only $\frac{2}{3}$ of the strength of the real one.

Coupled channels calculations were carried out for the measured elastic and inelastic cross sections using a deformed optical model potential of a form appropriate to a model of the target nuclei as axially symmetric rotors[15,16]

$$U = -(V_0 + iW_0)f(R') + V_c(R'), \tag{6}$$

$$f(R') = \frac{1}{1 + \exp[(R - R')/a]}, \tag{7}$$

where $R' = R_0(\Delta) + \delta_2(\Delta)Y_{20}(\theta, \phi) + \delta_4(\Delta)Y_{40}(\theta, \phi)$ depends on the polar angles (θ, ϕ) between the nuclear symmetry axis and a point on its surface. The undeformed radius $R_0(\Delta)$ is given as before by

$$R_0(\Delta) = r_0(A_t^{1/3} + A_p^{1/3}).$$

The symbol Δ indicates the target size. To lowest order in Δ/R_0, both R_0 and the deformation lengths $\delta_2(\Delta)$ and $\delta_4(\Delta)$ are independent of Δ.[8] The nuclear deformation β_2^n is obtained from $\delta_2(0) = \beta_2^n r_0 A_p^{1/3}$. The Coulomb potential in Eq. (6) is generated from

$$\rho(R', \theta) = \rho_0, \quad R' \leq R_c(\theta)$$
$$= 0, \quad R' > R_c(\theta), \tag{8}$$

where $R_c(\theta) = 1.2 A_p^{1/3}[1 + \beta_2^c Y_{20}(\theta, \phi)]$ and the charge density is normalized to $Z_p e$. The parametrization of R_c by $A_p^{1/3}$ rather than by $(A_p^{1/3} + A_t^{1/3})$ has been shown to yield a better description of the double-folded Coulomb potential of two heavy ions.[17]

The coupled-channels calculations were carried out using the same optical model parameters as used in the polarization potential calculations except that $\mathrm{Im}U_p = 0$. Initially only $0^+ - 2^+$ coupling with a quadrupole deformation was considered (i.e., $\delta_4 = 0$). The charge deformation parameters β_2^c of Eq. (8) were chosen to be consistent with $B(E2\uparrow)$ values which are related to charge densities by

$$[B(E2\uparrow)]^{1/2} = \int \rho(R', \theta) R^{1/2} Y_{20}(\theta, \phi) dR'. \tag{9}$$

The $B(E2)$ values used were the same as used in the polarization potential calculations. Equations (8) and (9) lead to $\beta_2^c = 0.498$ for ^{24}Mg and $\beta_2^c = 0.466$ for ^{28}Si. The coupled-channels calculations used the code *ECIS*[18] with 250 partial waves and radial integrations were carried out to 50 fm to account properly for Coulomb excitation. In order to test for convergence of the calculations, an additional calculation using the same parameter set was carried out for $^{28}Si + ^{208}Pb$ using 300 partial waves and integrating out to 70 fm. For angles greater than $\theta_{c.m.} = 35°$ the two calculations were the same to better than 0.1%. Because of the large expense involved in performing CC calculations, for the most part the optical model (OM) parameters were kept fixed. Calculations were made for a few values of β_2^n in an effort to try to optimize the fits to the 0^+ and 2^+ cross sections. In addition, for the $^{28}Si + ^{208}Pb$ cross sections the imaginary well depth W was varied in order to try to improve the fits to the cross section data. These calculations are shown in Figs. 2, 3, and 6–8 and are discussed below. In order to investigate the effect of hexadecapole deformation on the calculated cross sections a fit with $\beta_2 = 0.15$ and $\beta_4 = -0.05$ was performed for $^{24}Mg + ^{208}Pb$. This calculation is shown in Fig. 11.

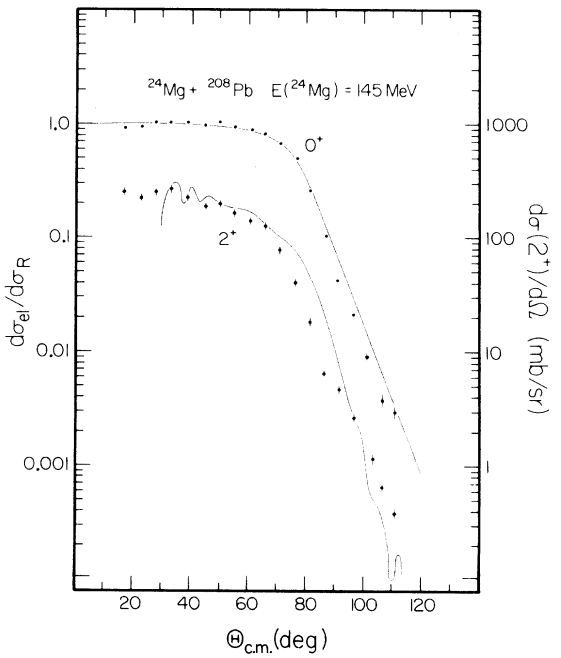

FIG. 6. Coupled channels calculations of the elastic and inelastic angular distributions for the $^{24}Mg + ^{208}Pb$ system at $E_{lab} = 145$ MeV using the optical model parameters of Table I, the experimental value of $B(E2)$, and a value of the nuclear deformation $\beta_2^n = 0.15$, are shown by the solid lines. See text for details.

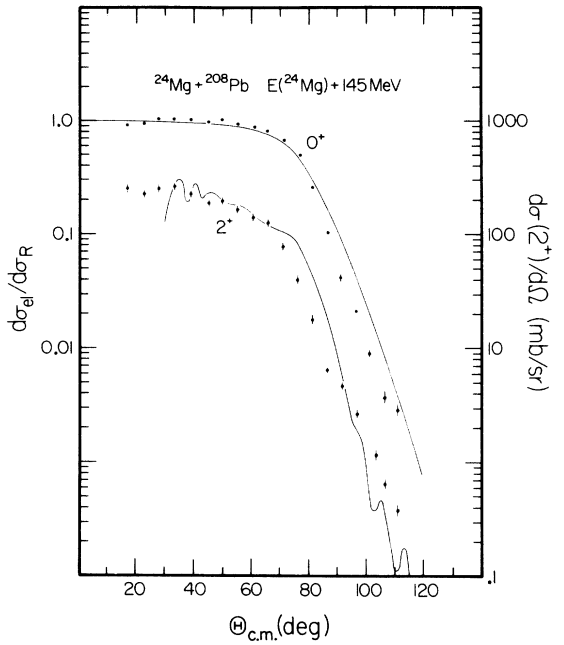

FIG. 7. Coupled channels calculations of the elastic and inelastic angular distributions for the $^{24}Mg + ^{208}Pb$ system at $E_{lab} = 145$ MeV using the optical model parameters of Table I, the experimental value of $B(E2)$, and a value of the nuclear deformation $\beta_2^n = 0.23$ are shown by the solid lines. See text for details.

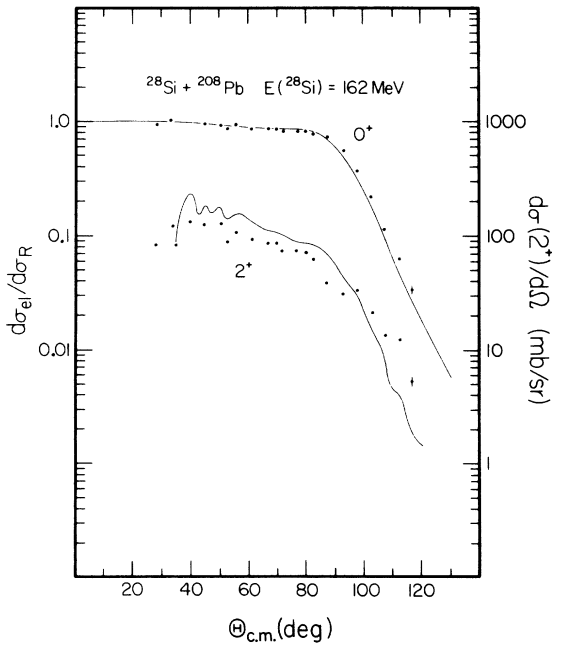

FIG. 8. Coupled channels calculations of the elastic and inelastic angular distributions for the $^{28}Si + ^{208}Pb$ system at $E_{lab} = 162$ MeV using the optical model parameters of Table I, the experimental value of $B(E2)$, and a value of the nuclear deformation parameter $\beta_2^n = -0.08$ are shown by the solid lines. See text for details.

IV. RESULTS

The optical model, which includes the polarization potential of Eqs. (3)–(5), yields a reasonably good fit to the measured elastic scattering cross sections when the experimental values for $B(E2)$ are used to calculate W_p. This is evidence of the fact that the main cause for the slow falloff from Rutherford scattering in the intermediate angular range, $40 \lesssim \theta_{c.m.} \lesssim 80$, is due to removal of flux from the elastic channel by Coulomb excitation of the lowest 2^+ state. If the inelastic scattering to the lowest 2^+ state is explicitly included in a coupled channels calculation, then, in principle, the same optical model potential used above with the polarization potential set equal to zero should yield a reasonable description of the elastic scattering cross sections if Coulomb excitation is the dominant mechanism for removing flux from the elastic channel at large impact parameters by population of the lowest 2^+ state. The ability of the CC calculations to describe the elastic scattering cross sections, especially in the intermediate angular range, is a good indication of the effectiveness of the polarization potential in simulating the effect of long range absorption on the elastic scattering cross sections.

For the case of $^{24}Mg + ^{208}Pb$ scattering, the optical potential of Table I with $U_p = 0$ was adopted in the coupled channels code and calculations were carried out for various values of β_2^n ranging from 0.0 to 0.30. Calculated cross sections for values of $\beta_2^n = 0.0$, 0.15, and 0.23 are shown in Figs. 2, 6, and 7, respectively. In all these cases $\beta_4 = 0$.

In general, the calculated cross sections, both the elastic and inelastic, are similar in shape to the measured cross sections. The calculated 2^+ cross sections are larger in magnitude than the measured 2^+ cross sections in the angular range from $\theta_{c.m.} = 70$–$100°$. For the case of $\beta_2^n = 0.0$ (i.e., only Coulomb excitation of the 2^+ state), the best fit is obtained to the elastic scattering cross section and the worst fit is obtained to the 2^+ cross section. As β_2^n is increased the magnitude of the calculated 2^+ cross section decreases in the angular range $\theta_{c.m.} = 40$–$100°$ and yields a slightly better description to the measured 2^+ cross section, but the fit to the elastic cross section deteriorates at the backward angles. As β_2^n is increased to values greater than 0.2, too much structure appears in the 2^+ cross section at backward angles and the fit to the elastic cross section continues to worsen. The best overall description to both the elastic and inelastic cross sections is obtained for $\beta_2^n = 0.15$. From the present analysis we conclude $\beta_2^n = 0.15 \pm 0.07$ where the large error arises from (a) neglect of the effects of hexadecapole coupling

(i.e., $\beta_4^n = 0$ in the present calculations) and (b) the fact that the contribution from the nuclear potential to excitation of the 2^+ state is small relative to the contribution of Coulomb excitation and therefore is very insensitive to the precise value of β_2^n. Using the approximate scaling rule of Hendrie[9]

$$\delta_2(\Delta) = \delta_2(0), \tag{10}$$

we can relate the potential deformation β_2^n to the intrinsic deformation of ^{24}Mg, $\beta_2^{^{24}\mathrm{Mg}}$.

$$\beta_2^n r_0 (A_T^{1/3} + A_p^{1/3}) = \beta_2^{^{24}\mathrm{Mg}} r_0 A_p^{1/3} \tag{11}$$

yields a value of $\beta_2^{^{24}\mathrm{Mg}} = 0.45 \pm 0.24$, in agreement with the results obtained by Thompson and Eck[9] from the analysis of the scattering of projectiles ranging in mass from $A = 1$–16 from ^{24}Mg.

For the case of the ^{28}Si + ^{208}Pb scattering cross sections, initial attempts to describe the data using the procedure outlined above (i.e., using the optical potential of Table I with $W_p = 0$) resulted in limited success. Calculations for $\beta_2^n = 0.0$, -0.08, and -0.15 are shown in Figs. 3, 8, and 9, respectively. The best fit to the elastic scattering cross section is obtained by $\beta_2^n = 0.0$. Decreasing β_2^n improves the fits to the 2^+ cross sections but causes serious discrepancies between the measured and calculated elastic cross sections in the backward

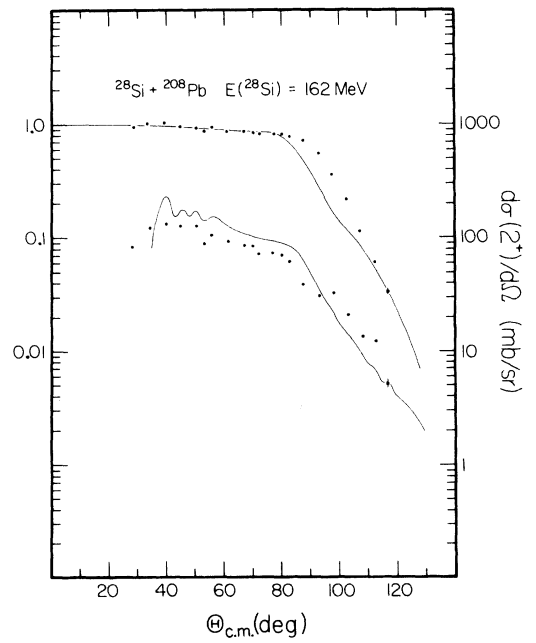

FIG. 9. Coupled channels calculations of the elastic and inelastic angular distributions for the ^{28}Si + ^{208}Pb system at $E_{lab} = 162$ MeV using the optical model parameters of Table I, the experimental value of $B(E2)$, and a value of the nuclear deformation parameter $\beta_2^n = -0.15$ are shown by the solid lines. See text for details.

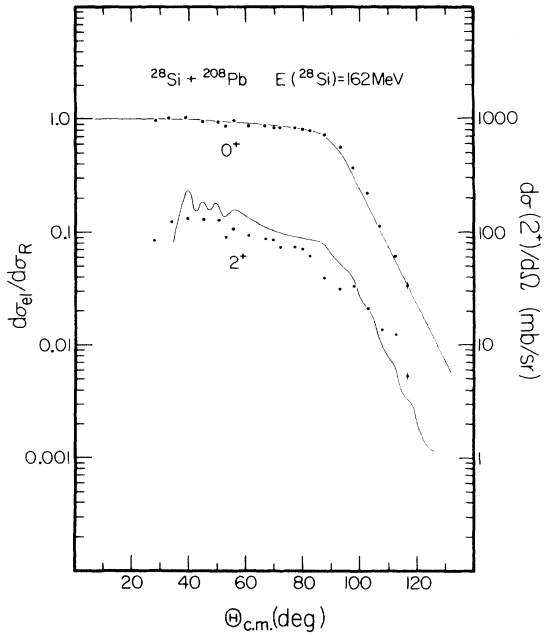

FIG. 10. Coupled channels calculations of the elastic and inelastic angular distributions for the ^{28}Si + ^{208}Pb at $E_{lab} = 162$ MeV using the optical model parameters of Table I with the exception that $W = 75$ MeV, the experimental value of $B(E2)$, and a value of $\beta_2^n = -0.08$ are shown by the solid lines. See text for details.

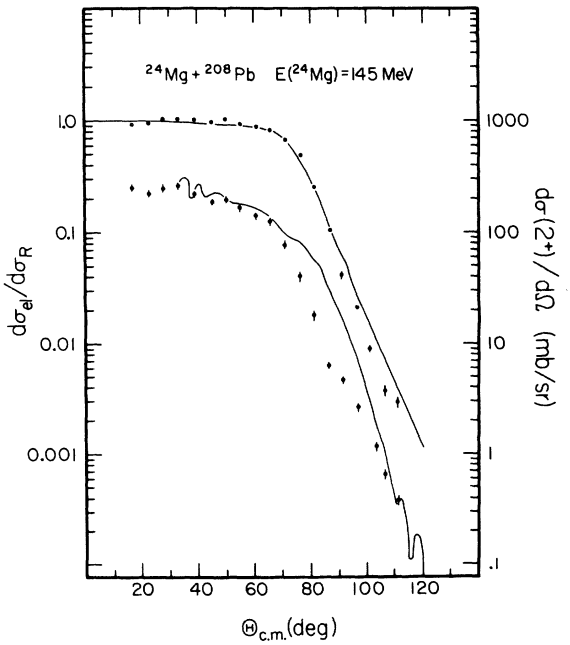

FIG. 11. Coupled channels calculations of the elastic and inelastic angular distributions for the ^{24}Mg + ^{208}Pb system at $E_{lab} = 145$ MeV using the optical model parameters of Table I, the experimental value of $B(E2)$, and the nuclear deformation parameters $\beta_2 = 0.15$ and $\beta_4 = -0.05$ are shown by the solid lines. See text for details.

angle region. In order to counter this tendency of the calculated elastic cross section to fall with decreasing β_2^n, the imaginary potential W was reduced. Reducing W and β_2^n allowed reasonable fits to be obtained to both the elastic and inelastic cross sections although the justification for this procedure is not really clear. The best fit obtained using this procedure is for $W=75.00$ MeV and $\beta_2^n=-0.08$ and is shown in Fig. 10. Because of the ambiguity in β_2^n and W it is difficult to determine β_2^n from the present work for ^{28}Si; however, the best estimate is $\beta_2^n=-0.08\pm0.08$ which, using Eq. (11), yields the intrinsic deformation of ^{28}Si as $\beta_2^{^{28}\mathrm{Si}}=-0.24\pm0.24$. The best value of $\beta_2^{^{28}\mathrm{Si}}$ obtained here is lower than the value obtained by Thompson and Eck[10] ($\beta_2=0.50\pm0.07$), but considering the large error in the present measurement is consistent with their value.

In order to evaluate the effect of the neglect of hexadecapole coupling in the above calculations the cross sections for ^{24}Mg + ^{208}Pb were calculated using the same optical model of Table I and $\beta_2=0.15$ and $\beta_4=-0.05$. This calculation is shown in Fig. 11. By comparison with Fig. 6 it can be seen that the effect of β_4 on the calculated cross sections is small and only changes the 2^+ cross section slightly in the angular range $\theta_{\mathrm{c.m.}}=80°-110°$. Because of the extremely high computing costs these calculations could not be pursued. The data presented here are available in tabulated form to those persons who might be interested in attempting a more thorough analysis.

V. CONCLUSIONS

Angular distributions for scattering to the ground and first excited 2^+ states of ^{24}Mg and ^{28}Si were measured for the ^{24}Mg + ^{208}Pb system at $E(^{24}\mathrm{Mg})=145$ MeV and for the ^{28}Si + ^{28}Pb system at $E(^{28}\mathrm{Si})=162$ MeV, respectively. Calculations using an optical model in conjunction with a polarization potential yielded a good description of the experimental cross sections and indicated the importance of Coulomb excitation in removing flux from the elastic scattering channel. Coupled channels calculations of both elastic and inelastic cross sections yielded a satisfactory overall description of the data but did not fit the details of the measured cross sections in any consistent way. Part of the reason for the inadequacy of present calculations can be attributed to (a) insensitivity to the nuclear deformation because of the strong contribution from Coulomb excitation and (b) the lack of any extended searching on the calculational parameters due to the excessive computing costs. Intrinsic deformation parameters for ^{24}Mg and ^{28}Si, obtained from scaling the potential deformation parameters of the coupled channels calculations, were consistent with previous work, although the errors of the present work make a detailed comparison impossible.

ACKNOWLEDGMENTS

This research was supported in part by the Division of Chemical Sciences, U.S. Department of Energy. One of the authors (J.S.E.) was supported in part by a grant from the U.S. National Science Foundation under the U.S.-Australia Cooperative Science Program.

[1]E. E. Gross, T. P. Cleary, J. L. C. Ford, D. C. Hensley, and K. S. Toth, Phys. Rev. C 17, 1665 (1978).
[2]Y. Lee, J. X. Saladen, J. Halden, J. O'Brien, C. Baktash, C. Bemis, Jr., P. H. Stelson, F. K. McGowan, W. T. Miller, J. L. C. Ford, Jr., R. L. Robinson, and W. Tuttle, Phys. Rev. C 12, 1483 (1975), and references therein.
[3]W. Brückmer, D. Husar, D. Pelte, K. Traxel, M. Samuel, and U. Smilansky, Nucl. Phys. A281, 159 (1974).
[4]J. X. Saladin, I. Y. Lee, R. C. Haight, and D. Vitoux, Phys. Rev. C 14, 992 (1976).
[5]D. S. Gale and J. S. Eck, Phys. Rev. C 7, 1950 (1973).
[6]John S. Eck, D. O. Elliott, W. J. Thompson, and F. T. Baker, Phys. Rev. C 16, 1020 (1977).
[7]F. Todd Baker, Alan Scott, E. E. Gross, B. C. Hensley, and D. L. Hillis, Nucl. Phys. A284, 135 (1977).
[8]D. L. Hendrie, Phys. Rev. Lett. 31, 478 (1973).
[9]W. J. Thompson and J. S. Eck, Phys. Lett. 67B, 151 (1977).
[10]W. G. Love, T. Terasawa, and G. R. Satchler, Nucl. Phys. A291, 183 (1977).
[11]T. R. Ophel and A. Johnston, Nucl. Instrum. Methods 157, 461 (1978).
[12]S. F. Biagi, W. R. Phillips, and A. R. Barnett, Nucl. Phys. A242, 160 (1975); D. Branford, A. C. McGough, and I. F. Wright, *ibid.* A241, 349 (1975); A. Nakada and Y. Torizuka, J. Phys. Soc. Jpn. 32, 1 (1972).
[13]Y. Horikawa, Prog. Theor. Phys. Jpn. 47, 867 (1972); P. M. Endt and C. van der Leun, Nucl. Phys. A214, 1 (1973).
[14]G. R. Satchler and W. G. Love, Phys. Rep. 55C, 183 (1979); G. R. Satchler, Nucl. Phys. A329, 233 (1979).
[15]A. Bohr and B. R. Mottelson, *Nuclear Structure* (Benjamin, Reading, Massachusetts, 1975), Vol. 2, p. 1.
[16]T. Tamura, Rev. Mod. Phys. 37, 678 (1965).
[17]J. Carter, R. G. Clarkson, V. Hnizdo, R. J. Deddy, and D. W. Mingay, Nucl. Phys. A273, 523 (1976).
[18]F. Todd Baker (private communication).